

## Article

# The Sulfide/Silicate Coefficients of Nd and Sm: Geochemical “Fingerprints” for the Syn- and Epigenetic Cu-Ni-(PGE) Ores in the NE Fennoscandian Shield

Pavel A. Serov \*  and Tamara B. Bayanova

Geological Institute of the Kola Science Centre, Russian Academy of Sciences, 184209 Apatity, Russia; tamara@geoksc.apatity.ru

\* Correspondence: serov@geoksc.apatity.ru

**Abstract:** One of the current directions of the Sm-Nd isotope systematics development is a dating of the ore process using sulfide minerals. Yet, the issue of the existence of rare earth elements (REE) in sulfides is still a matter for discussion. Sulfides from ore-bearing rocks of Proterozoic (2.53–1.98 Ga) Cu-Ni and platinum group elements (PGE) deposits of the Fennoscandian Shield were studied. It is found that the most probable source of REE in sulfide minerals from Cu-Ni-PGE complexes could be submicronic fluid inclusions, which are trapped at the mineral crystallization stage. In such a case, fluid or melt inclusions are specimens of the syngenetic parental melt, from which the base mineral formed, and these reflect a composition of the parental fluid. The mineral–rock partition coefficients for Nd and Sm can be used as “fingerprints” for individual deposits, and these are isotope-geochemical indicators of the ore-caused fluid that is syngenetic to sulfide. Moreover, the  $D_{Nd}/D_{Sm}$  ratio for various sulfide minerals can be used as a prospective geochemical tool for reconstructing a mineral formation sequence in ore complexes. On the other hand, differences in isotope compositions of sulfide neodymium could be markers of some ore-caused fluids and related to certain generations of sulfide minerals.

**Keywords:** sulfides; partition coefficients; REE distribution; fluid inclusions; Fennoscandian Shield; Cu-Ni-PGE ores



**Citation:** Serov, P.A.; Bayanova, T.B. The Sulfide/Silicate Coefficients of Nd and Sm: Geochemical “Fingerprints” for the Syn- and Epigenetic Cu-Ni-(PGE) Ores in the NE Fennoscandian Shield. *Minerals* **2021**, *11*, 1069. <https://doi.org/10.3390/min11101069>

## Academic Editors:

Antonios Koroneos, Ioannis Baziotis and Kristina Šarić

Received: 20 August 2021

Accepted: 27 September 2021

Published: 29 September 2021

**Publisher’s Note:** MDPI stays neutral with regard to jurisdictional claims in published maps and institutional affiliations.



**Copyright:** © 2021 by the authors. Licensee MDPI, Basel, Switzerland. This article is an open access article distributed under the terms and conditions of the Creative Commons Attribution (CC BY) license (<https://creativecommons.org/licenses/by/4.0/>).

## 1. Introduction

The samarium–neodymium system is one of the most demanded and informative isotope-geochronological tools for studying geological objects. It is successfully used for a wide age range, i.e., from the earliest point of Precambrian to Phanerozoic, and it provides reliable geochronological and geochemical data for different rock types. With accumulating knowledge on the behavior of REE in various geological processes, there is a matter of enhancing the Sm-Nd method capacity by using new minerals-geochronometers. One of the prospective areas is a dating of an ore process by the Sm-Nd method using sulfide minerals. A successful implementation of this approach on key ore objects of the Baltic Shield allowed defining major time points of ore formation of Proterozoic Cu-Ni-PGE complexes and geochronologically supports the conclusions that the ore process is syn- or epigenetic. The obtained Sm-Nd data are well-correlated with available U-Pb zircon and baddeleyite datings, which confirms the accuracy of the obtained results [1–5].

Yet, despite the prospectivity and relevance of this method, the issue of the existence REE in sulfides is still a matter for discussion. Some studies on REE in sulfides principally do not refute such a possibility [6–15]. A substantial part of literary data also point to a possible direct use of sulfide minerals for studying geological objects with a prevailing fluid–hydrothermal impact on concentration processes of ore-caused components [15–24]. In such a case, sulfide inherits parameters of the ore-bearing fluid, and it is syngenetic to this fluid. Works conducted during the past decade generally support these conclu-

sions [17,20–22,24–26]. Yet, in contrast to hydrothermal deposits, there are not enough similar studies for magmatic Cu-Ni-PGE complexes.

Our new data indicate a possible use of sulfides to determine the age of ore formation in mafic–ultramafic rocks, which allows extending the set of minerals suitable for the Sm-Nd method. The measured neodymium and samarium concentrations in the sulfides might be related to fluid or melt inclusions that reflect a composition of the parental ore-bearing melt. The determined coefficients of the sulfide/rock for Nd and Sm could be used as “fingerprints” for individual deposits, and they are some kinds of isotope–geochemical indicators of the ore-caused fluid that is syngenetic to the sulfide. Aside from that, the  $D_{Nd}/D_{Sm}$  ratio for various sulfide minerals can be used as a prospective geochemical tool for reconstructing a sequence of mineral formation in ore complexes.

## 2. Geological Settings

The Fennoscandian Shield hosts the vast Palaeoproterozoic East Scandinavian Mafic Large Igneous Province. Its current remnants cover about 1,000,000 km<sup>2</sup>. The shield basement formed as a mature Archaean granulite and gneiss–migmatite crust 2550 Ma ago. It is exposed in the Kola–Lapland–Karelia Craton. The main structural features of the East Scandinavian mafic Large Igneous Province and its Pd-Pt and Ni-Cu-PGE deposits are described in [27]. The exposed part of the shield extends beneath the sedimentary cover toward the northern Russian Platform as a vast Palaeoproterozoic Baltic–Mid-Russia wide arc-intracontinental orogen [28].

The long Early Palaeoproterozoic (2530–2400 Ma) geological history of the East Scandinavian mafic Large Igneous Province comprises several stages. They are separated by breaks in sedimentation and magmatic activity often marked by uplift erosion and the deposition of conglomerates. The Sumian stage (2550–2400 Ma) is crucial for the metallogeny of Pd-Pt ores. It can be related to the emplacement of high-Mg and high-Si boninite-like and anorthosite magmas [29,30]. The ore-bearing intrusions were emplaced in the Kola Belt (2530–2450 Ma) and in the Fenno-Karelian Belt (2450–2400 Ma) [2,3,5].

Recently, the Baltic Shield has been defined as the PGE-bearing East Scandinavian mafic Large Igneous Province of plume nature [2], or the Baltic Large Igneous Province with igneous rocks rich in Mg and Si [31], or the Kola–Lapland–Karelian plume province [32]. These Early Paleoproterozoic geological settings fill a substantial gap in the understanding of geological events and Pd-Pt and Ni-Cu metallogeny of the Late Neoproterozoic–Early Palaeoproterozoic transitional period in the Earth’s evolution (2.7–2.2 Ga ago). In classic metallogenic summaries [33–35], this period is characterized by the Stillwater, Great Dike of Zimbabwe, Bushveld, and Sudbury ore-bearing complexes. However, their geological setting cannot be coordinated in space and time with regional geological frameworks.

In the northeastern Baltic Shield (Figure 1), large-scale mafic–ultramafic deposits of Cu-Ni-Co, platinum group elements (PGE), and Fe-Ti-V are economically significant, in particular, concerning critical raw materials, such as PGE and V. These are major Cu-Ni-Co-Cr+PGE deposits in the Monchegorsk ore area [36–39] and Pechenga [40–42], Fe-Ti-V Kolvitsa deposit [43,44], PGE+Cu-Ni Fedorovo-Pansky layered complex [2,4,45,46], and Burakovsky intrusion [47], Cu-Ni-Co+PGE deposits in Finland: Kemi [39,48], Penikat [49], Portimo (Ahmavaara intrusion) [50,51], Akanvaara, Koitelainen [52], Tornio [51], etc.

The dated deposits were formed in two major episodes, at 2.53–2.39 Ga and 2.0–1.8 Ga, corresponding to the early [1,2,39,48,52–59] and late [40,42,60] stages of rifting in the Fennoscandian Shield.

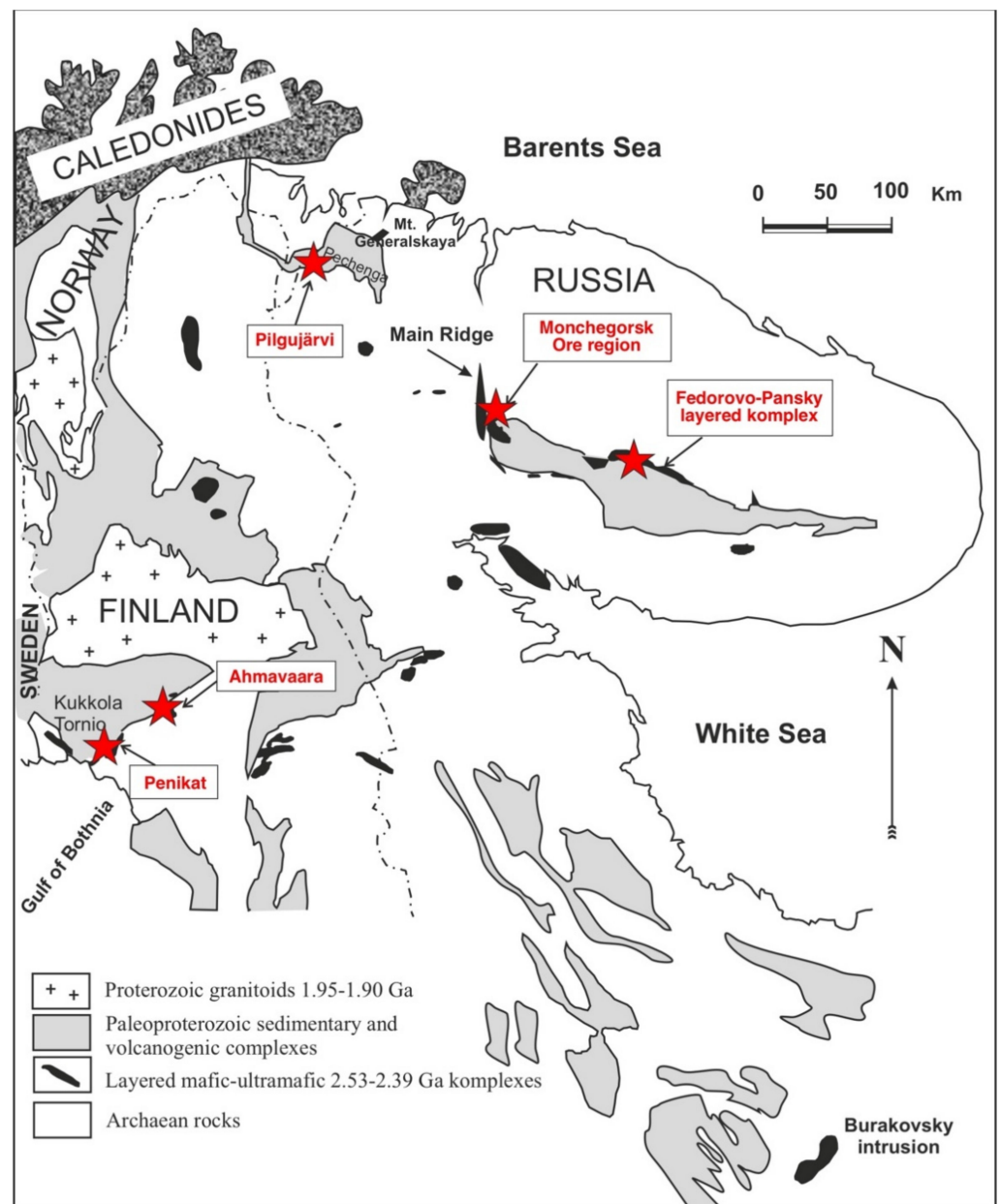


**Figure 1.** Generalized geological map of the northeastern part of the Baltic Shield and the location of Paleoproterozoic mafic layered intrusions (modified after [3]). Red asterisks indicate sampling locations.

### 2.1. Pilgijärvi 1.98 Ga Deposit (Pechenga Area)

The Pilgijärvi Cu-Ni deposit occurs in the central part of the Eastern ore field [60,61]. The genesis and distribution of ore bodies in the Pilgijärvi deposit is primarily related to the internal structure and tectonics of the main differentiated gabbro-peridotite massif notwithstanding the fact that this deposit accommodates more than a dozen other smaller nickel-bearing intrusive bodies with a similar composition. The internal structure of the massif demonstrates a primary banding of the composing rocks and ores. The ore body is mostly made up of crude impregnated ores (95%) with minor rich impregnated breccia and massive sulfide ores (ca. 5%). The constant confinement of the deposits to the peridotitic bottom parts of the differentiated intrusives, the sheet-like shape and occurrence of the majority of the ore bodies, and ore structures and textures imply a syngenetic nature of the overwhelming ore mass with respect to the mother rock. This is a reason why the

ore-forming process or the sulfide accumulation and segregation shall be considered as a phenomenon that accompanied the intrusive emplacement, differentiation, and chilling of the nickel-bearing magma at the turn of 1980 Ma [42].

### 2.2. Portimo 2.44 Ga Complex (Ahmavaara Intrusion)

The Portimo Complex accommodates the Ahmavaara, Narkaus, and Sukhanko-Konttijärvi intrusions with a crystallization age of 2.44 Ga, which presumably associate with a coeval dike swarm known as the Portimo dikes [51]. This complex is supposed to have formed at the expense of two various magmas with the early magma being richer in MgO, Cr, and LREE than the later one. Both magmas contained low TiO<sub>2</sub> (<0.5 wt %) and belong to the boninite series [62].

### 2.3. Monchegorsk 2.5 Ga Ore Field

The Monchegorsk ore field includes rocks of the ore-bearing layered Monchepluton, gabbro–anorthosite massifs of the Main Ridge (Monchetundra and Chunutundra), small intrusions of the Ostrovskoy massif and Yarva–Varaka, and dikes cutting through the Monchepluton [38,63,64]. The complex had been forming during a long period of time in the interval of 2.51–2.46 Ga [36,37,64].

At the modern erosional truncation, the Monchepluton has an arched shape and consists of two branches (or chambers). The northwestern branch is represented by the Nittis–Kumuzh’ya–Travyanaya (or NKT) massifs while the nearly east–west-trending one is composed of the Sopcha–Nyud–Poaz and Vurechuaivench massifs. The complex is made up of dunites, harzburgites, orthopyroxenites (NKT), orthopyroxenites (Sopcha), norites (Nyud), and gabbronorites (Poaz and Vurechuaivench) that form a single syngenetic rock series. It is distinctly differentiated both vertically and horizontally, which is generally expressed in the reduced rock basicity from the bottom up and from west to east [38,63,64].

### 2.4. Fedorovo-Pansky 2.5 Ga Layered Complex

The Fedorovo-Pansky layered complex occurs in the central part of the Kola Peninsula at a border between the Early-Proterozoic volcano-sedimentary rift series and Archean basement gneisses. The Fedorovo-Pansky complex mostly comprises gabbronorites with varying proportions of mafic minerals and different structural features. From the bottom up, the layered sequence is as follows [2,46]: Marginal Zone (50–100 m) of plagioclase–amphibole schists with relicts of massive fine-grained norite and gabbronorite, which are referred to as chilled margin rocks; Taxitic Zone (30–300 m), which contains an ore-bearing gabbronoritic matrix (2485 Ma) and early xenoliths of plagioclase-bearing pyroxenite and norite (2526–2516 Ma). Syngenetic and magmatic ores are represented by Cu and Ni sulfides with Pt, Pd, and Au, as well as Pt and Pd sulfides, bismuth–tellurides, and arsenides; Norite Zone (50–200 m) with cumulus interlayers of harzburgite and plagioclase-bearing pyroxenite that includes an intergranular injection Cu-Ni-PGE mineralization in the lower part.

## 3. Sulfide Geochronology of Cu-Ni-PGE Ore Deposits—Results of Previous Studies

For more than a decade, we have studied the main Cu-Ni-PGE deposits in the north-eastern part of the Fennoscandian Shield to determine the age of their ore formation. The main results are shown in Figure 2. It can be seen that sulfide minerals together with rock-forming minerals form good quality isochrones. This made it possible to determine the age of ore genesis for the main Cu-Ni-PGE ore deposits of the Fennoscandian Shield. In general, the Sm-Nd system of sulfide minerals is becoming a promising tool for studying ore processes. Along with syngenetic sulfides, young ages of redeposited and metamorphosed ores were also obtained for the Ahmavaara deposits (Finland) and the Monchegorsk region (Nyud-2). Further studies of the distribution of REEs in rocks and sulfides and their comparison led to important conclusions about isotopic fingerprints for syngenetic and

epigenetic ores. However, there are serious limitations and problems associated with the use of sulfides as geochronometers for the ore process (see Results and Discussion).

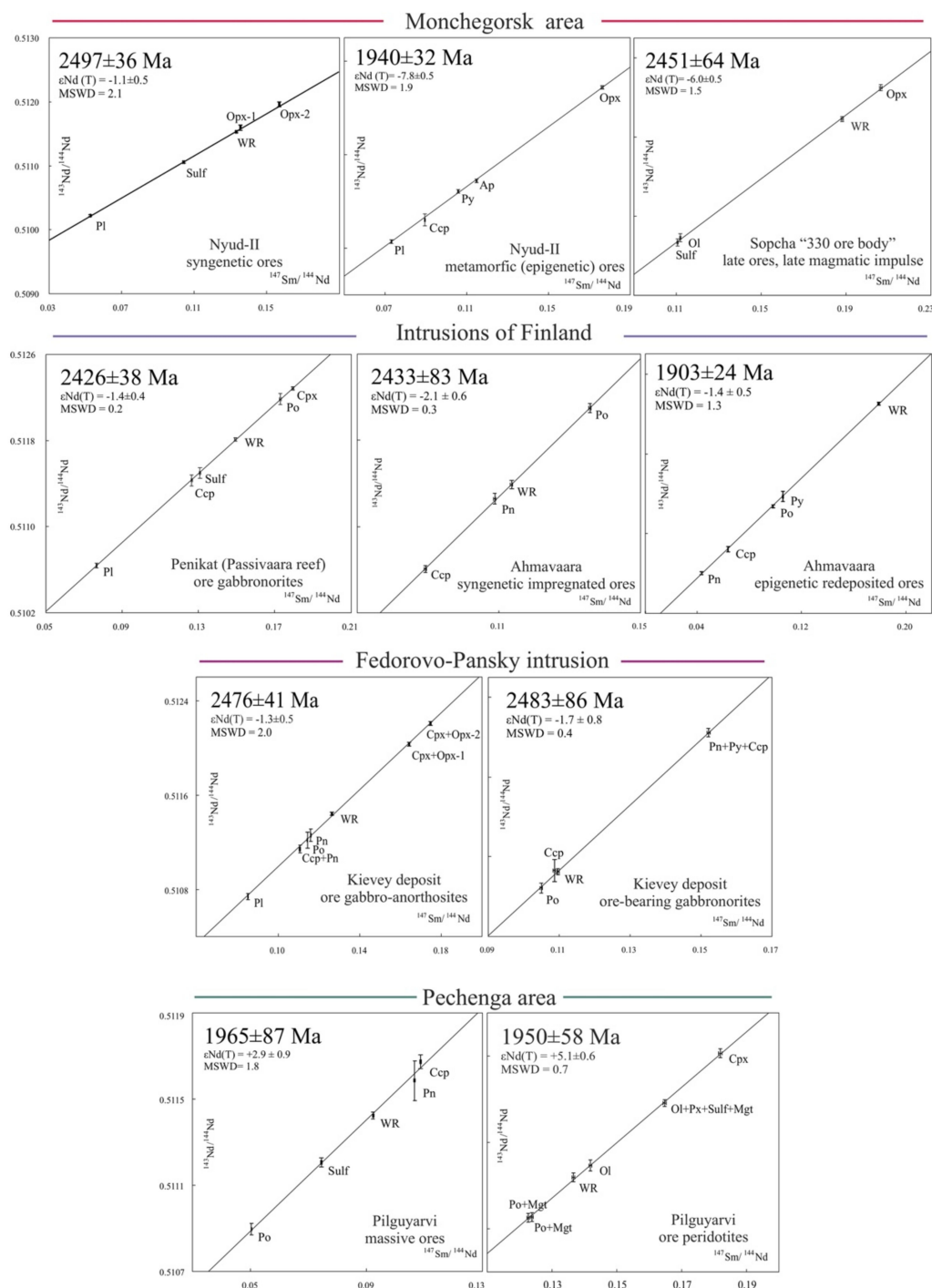


**Figure 2.** Mineral Sm-Nd isochrones for the main Cu-Ni-PGE ore deposits in the northeastern part of the Fennoscandian Shield. Data from [1–5].  $\epsilon_{Nd}(T)$ —isotopic composition of neodymium; MSWD—middle square weighted deviations. Minerals: Pl—plagioclase; Sulf—sulfide minerals mix; WR—whole rock; Po—pyrrhotite; Cpx—clinopyroxene; Opx—orthopyroxene; Ccp—chalcopyrite; Py—pyrite; Ap—apatite; Ol—olivine; Pn—pentlandite; Mgt—magnetite.

#### 4. Samples and Methods

Sulfides from Paleoproterozoic rocks (2.53–1.98 Ga) of Cu-Ni-PGE deposits of the Fennoscandian Shield were studied. The isotope research was carried out in the Collective

Use Centre of the Kola Science Centre RAS (Apatity, Russia). First, the samples were prepared by crushing; then, minerals were separated using heavy liquids, and mineral fractions were selected under binocular microscope.

#### 4.1. Sm-Nd Analytical Methods

In order to define concentrations of Sm and Nd, the sample was mixed with a compound tracer  $^{149}\text{Sm}/^{150}\text{Nd}$  prior to dissolution. Then, it was diluted with a mixture of HF + HNO<sub>3</sub> (or +HClO<sub>4</sub>) in Teflon sample bottles at a temperature of 100 °C until complete dissolution. Further extraction of Sm and Nd was carried out using standard procedures with two-stage ion-exchange and extraction–chromatographic separation using ion-exchange tar “Dowex” 50 × 8 in chromatographic columns employing 2.3 N and 4.5 N HCl as an eluent. The separated Sm and Nd fractions were transferred into a nitrate form, whereupon the samples (preparations) were ready for mass-spectrometric analysis.

The isotope Nd composition and Sm and Nd contents were measured at a 7-channel solid-phase mass-spectrometer Finnigan-MAT 262 (RPQ) in a static double-band mode, using Ta+Re filaments. A mean value of  $^{143}\text{Nd}/^{144}\text{Nd}$  ratio in a JNd<sub>i</sub>-1 standard was  $0.512081 \pm 13$  (N = 11) in the test period. An error in  $^{147}\text{Sm}/^{144}\text{Nd}$  in ratios was 0.3% (2σ), which is a mean value for 7 measurements in a BCR-2 standard [65]. An error in estimation of isotope Nd composition in an individual analysis was up to 0.01% for minerals with low Sm and Nd contents. The blank intralaboratory contamination was 0.3 ng in Nd and 0.06 ng in Sm. The accuracy of estimation of Sm and Nd contents was ±0.5%. Isotope ratios were normalized per  $^{146}\text{Nd}/^{144}\text{Nd} = 0.7219$  and then recalculated for  $^{143}\text{Nd}/^{144}\text{Nd}$  in JNd<sub>i</sub>-1 = 0.512115 [66].

#### 4.2. Study of Sulfide Mineral Texture

Sulfides were studied using back-scattered electrons with a high-performance LEO 1450 scanning electron microscope. Analyses were carried to study possible inclusions in sulfides with considerable concentrations of REE that might have distorted results of Sm-Nd dating [67]. A preliminary study of sulfide minerals using BSE allowed finding small silicate microinclusions (Figure 3), which cannot have a substantial impact on the results of the Sm-Nd analysis.

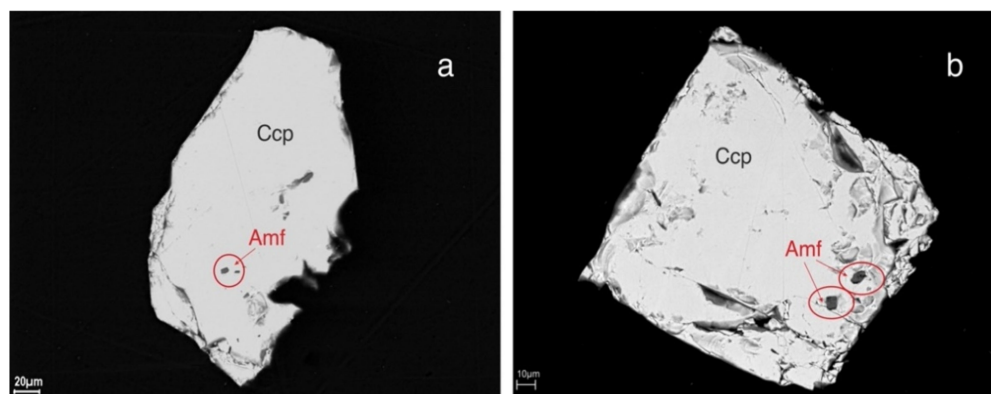


**Figure 3.** Silicate microinclusions (amphibole) in chalcopyrite from the Penikat intrusion (a) and the Fedorovo-Pansky complex (b).

Moreover, to provide a higher study accuracy, the sulfides were sampled manually under a binocular microscope to discard minerals with visible microinclusions.

#### 4.3. ICP-MS

To define REE in samples with no preliminary separation and concentration, reference values of REE concentrations in the GSO 2463 Standard (apatite), sulfide from the Talnakh deposit, and international standard samples of the Centre of Petrographic and Geochemical

Research (Nancy, France) were reproduced using the ELAN 9000 DRC-e (Perkin Elmer, Waltham, MA, USA) quadrupole mass-spectrometer in Tananaev Institute of Chemistry KSC RAS (Apatity, Russia). The samples were separated under the conditions provided in [67].

The analysis was based on the following parameters: plasma power of 1300–1350 W; sprayer gas flow (high-clean Ar) within 0.75–1.0 L/min<sup>-1</sup>; ion lens voltage <11 V; and level of doubly charged and oxide ions <2.5%. A geological sample weighing up to 100 mg in the polystyrene hermetically sealed test tube mixed with distilled acids (HNO<sub>3</sub>, HF, HCl 5 mL each) was exposed to water bath at a temperature of 50–60 °C until fully dissolved. No HCl was added in the course of opening of sulfide minerals. When opening the sample, we have registered an increased pressure of acid and nitrogen oxide vapor that suppressed the volatility of the components in the sample. The chilled sample was mixed with 0.1 mL H<sub>2</sub>O<sub>2</sub>, and the dissolved sample was diluted with 2% HNO<sub>3</sub>. The level of total REE content in the blank sample was <0.5 ppb. This blank sample qualifies the level of analytical accuracy and limit of element detection. Since the samples have yielded high concentrations of those elements that may cause a matrix effect and ion interference, the calibration curves were plotted with interfering agent added to the blank calibration solution. The multicomponent standard solutions by Perkin Elmer (Multi-element ICP-MS Calibration Std, Waltham, MA, USA) were used. The sample itself was selected as an interfering agent. The amount of the interfering agent was chosen so that the macrocomponent concentration after mixing exceeded the REE concentration in the calibration solution by a factor of 100. The approximation linearity of the REE correction curves is ≥99.99%. Spectral superimposition was recognized by ELAN 9000 DRC-e MS software (Perkin Elmer, Waltham, MA, USA) and adjusted by the introduction of correction equations into the analytic program defined with reference to a natural abundance of REE isotopes. The blank sample solution free of the interfering agent was used to analyze the solution of the opened sample.

## 5. Results and Discussion

A total of 34 monofractions of sulfide minerals from Paleoproterozoic-layered complexes of the Fennoscandian Shield were studied using mass spectrometry (Table 1).

**Table 1.** Results of analytical Sm-Nd research of sulfide minerals from mafic–ultramafic complexes of the Fennoscandian Shield and calculated sulfide/rock partition coefficients for Nd and Sm.

Sample	Sulfide Type	Rock and Geological Setting	Concentrations in Sulfide, ppm		Concentrations in Whole Rock (WR), ppm		D <sub>Sm</sub>	D <sub>Nd</sub>	D <sub>Nd</sub> / D <sub>Sm</sub>
			Sm	Nd	Sm	Nd			
B58/111	mix	plagioclase (Monchegorsk area)	0.030	0.120	0.970	4.620	0.030	0.025	0.83
P-1/109	mix	orthopyroxenite (Monchetundra)	0.032	0.123	0.678	2.090	0.047	0.058	1.23
MT-3	mix	orthopyroxenite (Monchetundra)	0.020	0.090	0.245	1.055	0.081	0.085	1.05
B70/111	mix	olivine orthopyroxenite (Monchegorsk area)	0.034	0.188	0.041	0.131	0.829	1.435	1.73
Pilg-4/3	mix	massive ore (Pilgajärvi, Pechenga)	0.070	1.050	0.260	1.700	0.269	0.617	2.29
F-4	mix	gabbronorite (Penikat)	0.114	0.709	2.000	10.07	0.057	0.070	1.23
F-8	mix	gabbronorite (Penikat)	0.008	0.038	0.710	2.870	0.011	0.013	1.18
FPM-1 Ccp+Pn	mix	gabbronorite (Fedorovo-Pansky complex)	0.022	0.122	1.044	4.994	0.021	0.024	1.14
FPM-1 Pn+Py+Ccp	mix	gabbronorite (Fedorovo-Pansky complex)	0.424	1.663	0.563	3.120	0.753	0.533	0.71
BGF-616 Py+Pn	mix	gabbro (Fedorovo-Pansky complex)	0.153	0.912	1.313	5.770	0.116	0.158	1.36
P-1/109 Po	pyrrhotite	orthopyroxenite (Monchetundra)	0.018	0.095	0.678	2.090	0.026	0.045	1.73
Pilg-4/3 Po	pyrrhotite	massive ore (Pilgajärvi, Pechenga)	0.180	2.180	0.260	1.700	0.692	1.282	1.85
F-4 Po	pyrrhotite	gabbronorite (Penikat)	0.301	2.020	2.000	10.07	0.151	0.200	1.32
MP-1 Po	pyrrhotite	gabbronorite (Fedorovo-Pansky complex)	0.029	0.151	1.044	4.994	0.027	0.030	1.11

Table 1. Cont.

Sample	Sulfide Type	Rock and Geological Setting	Concentrations in Sulfide, ppm		Concentrations in Whole Rock (WR), ppm		D <sub>Sm</sub>	D <sub>Nd</sub>	D <sub>Nd</sub> /D <sub>Sm</sub>
			Sm	Nd	Sm	Nd			
FPM-1 Po	pyrrhotite	gabbronorite (Fedorovo-Pansky complex)	0.028	0.176	0.563	3.120	0.049	0.056	1.14
FPM-1 Po-2	pyrrhotite	gabbronorite (Fedorovo-Pansky complex)	0.073	0.294	1.132	6.010	0.064	0.048	0.75
F-27 Po	pyrrhotite	redeposited ores (Ahmavaara)	0.263	1.617	2.490	8.410	0.105	0.192	1.83
B58/111 Pn	pentlandite	plagioclase (Monchegorsk area)	0.109	0.350	0.970	4.620	0.112	0.075	0.67
Pilg-4/3 Pn	pentlandite	massive ore (Pilgajärvi, Pechenga)	0.040	0.210	0.26	1.700	0.153	0.123	0.80
F-8 Pn	pentlandite	gabbronorite (Penikat)	0.005	0.017	0.710	2.870	0.007	0.005	0.71
F-8 Pn	pentlandite	gabbronorite (Penikat)	0.008	0.044	1.044	4.994	0.008	0.008	1.00
F-28 Pn	pentlandite	massive ores (Ahmavaara)	0.151	0.842	1.132	6.010	0.133	0.140	1.05
F-27 Pn	pentlandite	redeposited ores (Ahmavaara)	0.192	4.990	2.490	8.410	0.077	0.593	7.70
Pilg-4/3 Ccp	chalcopyrite	massive ore (Pilgajärvi, Pechenga)	0.040	0.230	0.260	1.700	0.153	0.135	0.88
F-4 Ccp	chalcopyrite	gabbronorite (Penikat)	0.109	0.647	2.10	10.07	0.054	0.064	1.19
F-8 Ccp	chalcopyrite	gabbronorite (Penikat)	0.005	0.019	0.710	2.870	0.007	0.006	0.86
FPM-1 Ccp	chalcopyrite	gabbronorite (Fedorovo-Pansky complex)	0.049	0.248	0.563	3.120	0.087	0.079	0.91
BGF-616 Ccp	chalcopyrite	gabbro (Fedorovo-Pansky complex)	0.104	0.597	1.313	5.770	0.079	0.103	1.30
F-28 Ccp	chalcopyrite	massive ores (Ahmavaara)	0.761	5.140	1.132	6.010	0.672	0.855	1.27
F-27 Ccp	chalcopyrite	redeposited ores (Ahmavaara)	0.183	3.040	2.490	8.410	0.073	0.361	4.95
F-4 Py	pyrite	gabbronorite (Penikat)	0.117	0.767	2.000	10.07	0.058	0.076	1.31
F-6 Py	pyrite	gabbronorite (Penikat)	0.417	1.706	0.850	4.410	0.490	0.386	0.79
BGF-616 Py	pyrite	gabbro (Fedorovo-Pansky complex)	0.082	0.452	1.313	5.770	0.062	0.078	1.26
BGF-616 Py	pyrite	gabbro (Fedorovo-Pansky complex)	0.157	0.934	2.490	8.410	0.063	0.111	1.76

The partition coefficients were calculated according to the equations:  $D_{Nd} = [Nd]_{Sulf} / [Nd]_{WR}$ ;  $D_{Sm} = [Sm]_{Sulf} / [Sm]_{WR}$ ; where  $D_{Nd}$  and  $D_{Sm}$  are the sulfide/rock partition coefficients for neodymium and samarium;  $[Nd]_{Sulf}$  and  $[Sm]_{Sulf}$ —concentration of neodymium and samarium in sulfide;  $[Nd]_{WR}$  and  $[Sm]_{WR}$ —concentration of neodymium and samarium in the whole rock (WR).

Sulfide/rock partition coefficients for neodymium vary from 0.076 to 0.386 for pyrite; from 0.006 to 0.855 for chalcopyrite; from 0.005 to 0.593 for pentlandite; and from 0.030 to 1.282 for pyrrhotite. The sulfide/rock partition coefficients for samarium vary from 0.062 to 0.490 for pyrite; from 0.007 to 0.672 for chalcopyrite; from 0.007 to 0.153 for pentlandite; and from 0.026 to 0.692 for pyrrhotite. Partition coefficients of Nd and Sm were determined (Table 1): for pyrite—0.229 and 0.169, respectively; for pyrrhotite—0.265 and 0.160; for chalcopyrite—0.229 and 0.161; for pentlandite—0.158 and 0.082. Mean values are  $D_{Nd} = 0.223$ ,  $D_{Sm} = 0.159$ . The  $D_{Nd}/D_{Sm}$  ratio increases in the pyrite–chalcopyrite–pyrrhotite–pentlandite sequence from 0.96 for pyrite to 1.93 for pentlandite (Table 2). A mean value of the  $D_{Nd}/D_{Sm}$  ratio is 1.40 for all the minerals studied.

**Table 2.** Sulfide/rock partition coefficients of neodymium ( $D_{Nd}$ ) and samarium ( $D_{Sm}$ ) in sulfides.  $N_{samp}$ —number of analyzed concentrates.

Sulfide Type	$D_{Nd}$	$D_{Sm}$	$D_{Nd}/D_{Sm}$	$N_{samp}$
pyrite	$0.163 \pm 0.020$	$0.169 \pm 0.005$	0.96	4
chalcopyrite	$0.229 \pm 0.017$	$0.161 \pm 0.003$	1.42	7
pyrrhotite	$0.265 \pm 0.015$	$0.160 \pm 0.003$	1.65	7
pentlandite	$0.158 \pm 0.015$	$0.082 \pm 0.003$	1.93	6
mix	$0.302 \pm 0.010$	$0.222 \pm 0.004$	1.36	10
Mean	$0.223 \pm 0.015$	$0.159 \pm 0.004$	1.40	

In general, the observed variations in values are quite wide, but the  $D_{Nd}/D_{Sm}$  ratio is more stable. Most of the  $D_{Nd}/D_{Sm}$  values are within the 0.70–1.70 range. Only for redeposited or metamorphosed ores, this ratio is sharply increased and varies from 2.30 to 7.70. At the same time, on the diagram in  $D_{Nd}$ – $D_{Sm}$  coordinates (Figure 4), sulfide points form a distinct trend, reflecting the relationship between the Nd and Sm partition coefficients. The sulfide figurative points from the redeposited Ahmavaara ores, the

massive Pilgujärvi ores, and the metamorphized ores of the Nyud-2 deposit are located above the trend line. The greater mobility of neodymium as compared to samarium during superimposed processes probably affects the redistribution of Nd by rock and sulfide, causing an increase in the partition coefficient. Thus, due to the epigenetic process, the  $D_{Nd}/D_{Sm}$  ratio tends to increase.

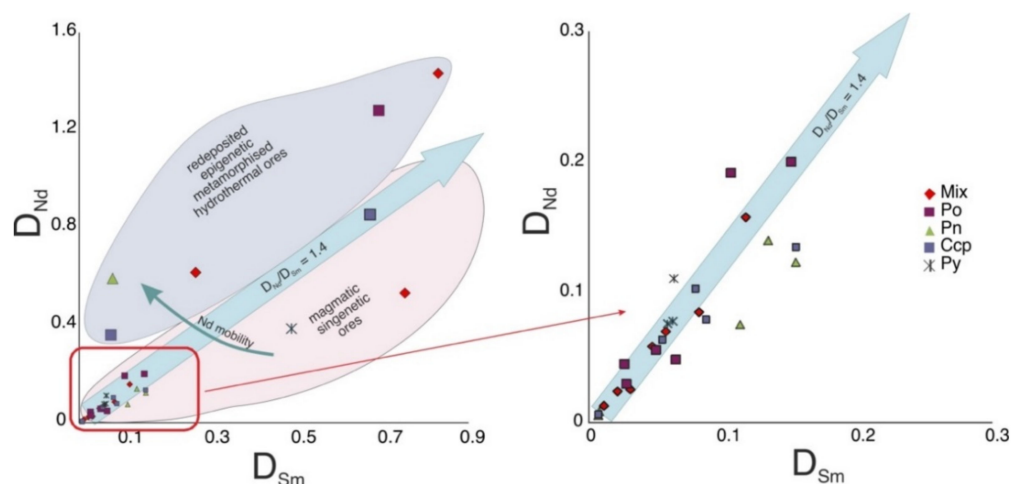


**Figure 4.** Partition coefficients  $D_{Nd}$ - $D_{Sm}$  in various sulfide minerals from Cu-Ni-PGE complexes of the Fennoscandian Shield. Mix—mixture of sulfide concentrates, Po—pyrrhotite, Pn—pentlandite, Ccp—chalcopyrite, Py—pyrite.

There are a few hypotheses on existing REE in sulfide minerals: isomorphic substitution of major cations [11,68]; silicate microinclusions [9,69]; defects of mineral crystalline lattice [70]; sorption on mineral surfaces [13]; and fluid inclusions in sulfides with the inherited REE composition from the ore-bearing melt [21–23].

Despite the fact that finding REE in sulfide minerals is contentious, different researchers are sufficiently confident to suggest that the type of REE partition in sulfides is inherited from the ore-bearing fluid, impacting the formation of sulfide minerals. Our studies (Figure 5, Table 3) on the partition of REE in the sulfides from ores of the Pilgujärvi deposit (Pechenga) and the Penikat intrusion (Finland) revealed that the type of REE partition in sulfides repeats the REE partition in the rock [71].

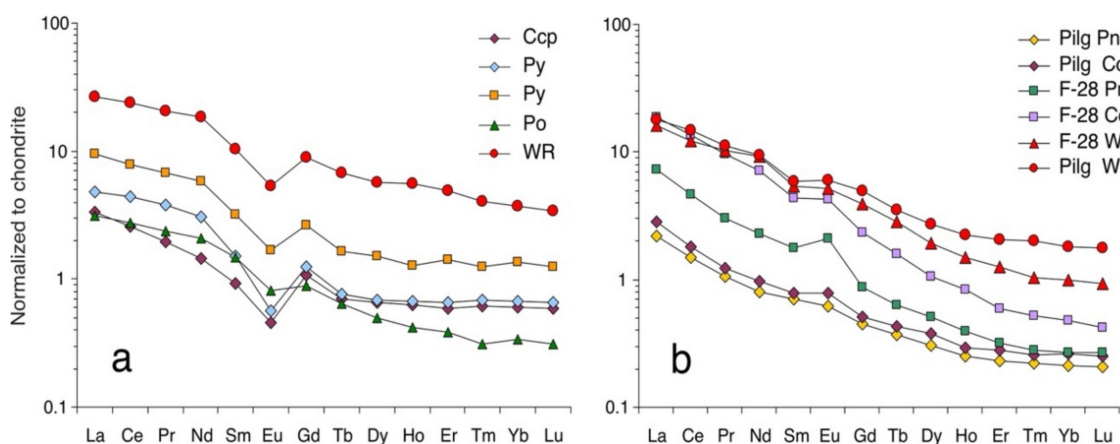


**Figure 5.** REE distribution in a rock (WR) and sulfide minerals from Cu-Ni-PGE complexes of Fennoscandian Shield: 2.44 Ga Penikat intrusion (a) and 1.98 Ga Pilgujärvi deposit (Pechenga) (b).

**Table 3.** ICP-MS data for rocks (WR) and sulfide minerals from Cu-Ni-PGE complexes of Fennoscandian Shield.

Sample	Concentrations, ppm													
	La	Ce	Pr	Nd	Sm	Eu	Gd	Tb	Dy	Ho	Er	Tm	Yb	Lu
	<b>Penikat</b>													
Ccp	1.03	2.077	0.24	0.863	0.18	0.03	0.28	0.033	0.21	0.045	0.12	0.02	0.127	0.019
Py	1.49	3.582	0.464	1.838	0.30	0.04	0.32	0.036	0.22	0.048	0.14	0.022	0.14	0.021
Py	2.93	6.371	0.823	3.524	0.62	0.12	0.69	0.078	0.48	0.092	0.3	0.04	0.282	0.04
Po	0.97	2.24	0.29	1.26	0.29	0.06	0.23	0.03	0.16	0.03	0.08	0.01	0.07	0.01
WR	8.31	19.192	2.533	10.97	2.02	0.4	2.31	0.32	1.83	0.401	1.03	0.131	0.77	0.11
	<b>Pilgijärvi</b>													
Pilg Pn	0.677	1.203	0.130	0.477	0.137	0.046	0.116	0.017	0.099	0.018	0.048	0.007	0.045	0.007
Pilg Ccp	0.878	1.453	0.149	0.583	0.154	0.058	0.132	0.020	0.122	0.021	0.059	0.008	0.055	0.008
Pilg WR	5.532	11.881	1.354	5.671	1.156	0.445	1.297	0.165	0.881	0.160	0.435	0.065	0.382	0.056
	<b>Ahmavaara</b>													
F-28 Pn	2.261	3.787	0.370	1.370	0.344	0.155	0.224	0.030	0.164	0.029	0.067	0.009	0.056	0.009
F-28 Ccp	5.862	11.066	1.171	4.300	0.853	0.314	0.605	0.075	0.340	0.060	0.125	0.017	0.100	0.014
F-28 WR	5.025	9.854	1.264	5.518	1.063	0.386	1.006	0.134	0.626	0.108	0.265	0.034	0.209	0.030

Analogous patterns of REE partition are detected in sulfides and many hydrothermal deposits, for which a role of fluids in ore genesis is defining [19,23]. Therefore, the most probable source of REE in the studied sulfides is heterogeneous fluid or melt inclusions occurring as submicronic bubbles. Additional arguments in favor of this suggestion are studies on silicate microinclusions in sulfides as a possible REE source. It was determined that the REE composition of silicate microinclusions is part of the overall REE balance of the fluid from which the sulfide crystallized. Thus, the total REE composition in a mineral can be taken as a reflection of the ore-forming fluid composition [9,69]. From a practical point of view, in terms of the Sm-Nd method, this means that the position of the sulfide points on the isochron will be controlled by different distribution coefficients of Nd and Sm, which is associated with different fluid inclusions. However, these inclusions are syngenetic to sulfide and rock-forming minerals. Therefore, sulfides can be used to determine the age of ore genesis, along with rock-forming minerals.

One of the issues on REE behavior in magmatic systems of Cu-Ni-PGE deposits is to determine a possibility that there are REE-bearing fluids at temperatures of the magmatic process. A hydrothermal process is characterized by much lower temperatures (generally lower than 400–450 °C) compared to temperatures for the crystallization of magmatic sulfides of Cu-Ni-PGE complexes, i.e., more than 1000 °C. Yet, studies on heterophase fluid inclusions in rocks of the Merensky reef (Bushveld) justify a presence of the ore-bearing fluid at temperatures of 900 °C and higher [72,73]. This means that already at temperatures of sulfide formation, ore fluid exists that can be captured by sulfide in the form of submicron inclusions.

Taking into account the arguments presented, the most probable source of REE in sulfide minerals from Cu-Ni-PGE complexes can be submicronic fluid inclusions, which are trapped at the early stage of mineral crystallization. In this case, fluid or melt inclusions are specimens of the syngenetic parental melt, from which the base mineral crystallized, and reflect a composition of the parental fluid. Thus, the determined coefficients of the mineral/rock partition for Nd and Sm will characterize a genesis of ore matter of a certain deposit and define isotope indicators (fingerprints) of the ore process. Moreover, they provide isotope-geochemical data on the ore-forming fluid and allow dating the ore process directly. The  $D_{Nd}/D_{Sm} = 1.4$  ratio obtained for all of the minerals is well-correlated with the interval of values obtained in the work [74], where a dependence of partition coefficients on FeO content and temperature is shown based on an experiment with sulfides under

reduction conditions. It is found that if the temperature decreases from 2100 to 1400 °C at 1.5 GPa, the  $D_{Nd}/D_{Sm}$  ratio tends to be in the range of 1.3–1.5. For natural sulfides, it can underlie different partition coefficients depending on the temperature occurring when cooling and their sequential formation.

E.g., for massive syngenetic ores of Ahmavaara, the  $D_{Nd}/D_{Sm}$  ratio is, on average, 1.3, while for the redeposited ore, the  $D_{Nd}/D_{Sm}$  ratio increases up to 4.8 (Table 1). It can indicate a significant hydrothermal impact leading to an increase in neodymium mobility and its migration of diffusion into fluid inclusions of the sulfide (Figure 4). The consequence of this is a relative accumulation of neodymium as compared to samarium and the increasing  $D_{Nd}/D_{Sm}$  ratio. By contrast, for ore gabbro-norites of the Penikat intrusion and the Fedorovo-Pansky layered complex, the  $D_{Nd}/D_{Sm}$  ratio shows a rather narrow range of values, i.e., 1.2–1.3 (Table 1). Along with similar Sm-Nd (sulfide) and U-Pb ages, it indicates a syngenetic genesis of the sulfides and rocks of the complexes, which is testified by geological and mineralogical observations.

Apart from it, a trend of the increasing  $D_{Nd}/D_{Sm}$  ratio in the pyrite–chalcopyrite–pyrrhotite–pentlandite sequence was determined (Figure 6, Table 2).

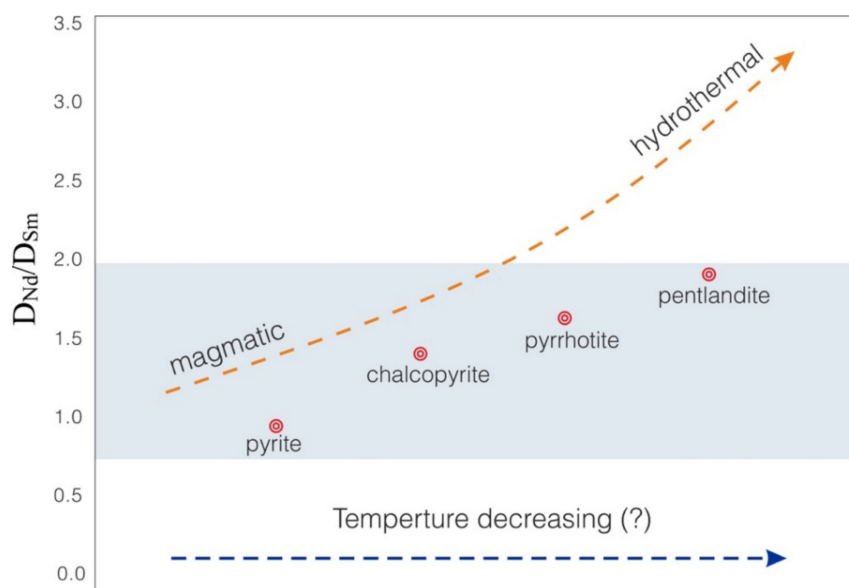


**Figure 6.**  $D_{Nd}/D_{Sm}$  ratio trend in the pyrite–chalcopyrite–pyrrhotite–pentlandite sequence. Higher values of this ratio are found for epigenetic or hydrothermal ores. This may be due to the hydrothermal processes of sulfide redeposition or the influence of a late fluid with different geochemical characteristics. An increase in the  $D_{Nd}/D_{Sm}$  ratio is also likely associated with a melt temperature decreasing and can be used to reconstruct the sequence of sulfide crystallization. Dotted arrow indicates an estimated decreasing trend in temperature.

This offers prospects for reconstructing a possible sequence of sulfide crystallization and defining conditions for ore formation in intrusive complexes of different age and genesis. Using these new data, it seems intuitively reasonable to implement the obtained results for analyzing other deposits, e.g., three stages of mineral formation with the pyrite–chalcopyrite–pyrrhotite–pentlandite sequence were defined for the Kun-Manye Cu-Ni deposit (Russia) [75]. For the Irankuh Zn-Pb deposit (Iran), a pyrite–chalcopyrite sequence of ore mineral formation is also defined [24]. The analysis of the  $D_{Nd}/D_{Sm}$  ratios for sulfides of various genesis shows that values of  $D_{Nd}/D_{Sm}$  increase for minerals of later processes, which correspond to ore redeposition or hydrothermal impact. Moreover, different isotope compositions of sulfide neodymium can be indicators of ore-caused fluids and related to certain generations of sulfide minerals, as shown for the Bathtub intrusion, Duluth Complex [76]. Yet, the issues related to the numerous episodes of hydrothermal processes

or influence of some fluids with various isotope characteristics during the ore formation are being extensively studied [76–79].

## 6. Conclusions

In general, the proposed approach considerably extends the available tool set of the Sm–Nd method. Apart from isotope-geological data, the results of the conducted study provide additional geochemical data on ore genesis processes at sulfide mineral crystallization stages, as well as at the following stages of hydrothermal impact.

Therefore:

- (1) The  $D_{Nd}$  and  $D_{Sm}$  partition coefficients were determined for various sulfide types, which is consistent with the experimental data;
- (2) The most probable REE source of sulfides is an ore-forming fluid appearing at the very stage of formation of sulfides from the melt at temperatures above 900 °C;
- (3) Prospects for defining a possible sequence of sulfide crystallization and reconstructing ore formation conditions in intrusive complexes of different ages were studied;
- (4) Differences in isotope compositions of sulfide neodymium could be indicators of some ore-caused fluids and related to certain generations of sulfide minerals.

**Author Contributions:** Conceptualization, P.A.S. and T.B.B.; methodology, P.A.S.; investigation, P.A.S. and T.B.B.; resources, T.B.B.; data curation, P.A.S. and T.B.B.; writing—original draft preparation, P.A.S.; writing—review and editing, P.A.S. and T.B.B.; visualization, P.A.S.; supervision, P.A.S. and T.B.B.; project administration, T.B.B.; funding acquisition, T.B.B. All authors have read and agreed to the published version of the manuscript.

**Funding:** The paper has been implemented in the framework of the Scientific Research Contract of GI KSC RAS 0226-2019-0053 and partly funded by the Russian Foundation for Basic Research 18-05-70082.

**Acknowledgments:** The authors thank O.G. Sherstenikova and N.A. Ekimova (GI KSC RAS) for their help in the chemical preparation of rocks; L.M. Lyalina (GI KSC RAS) for her assistance in studying the structure of the minerals; L.I. Koval (GI KSC RAS) for extraction of mineral fractions and grinding of rocks.

**Conflicts of Interest:** The authors declare no conflict of interest.

## References

1. Serov, P.A.; Bayanova, T.B.; Steshenko, E.N.; Kunakkuzin, E.L.; Borisenko, E.S. Metallogenic Setting and Evolution of the Pados-Tundra Cr-Bearing Ultramafic Complex, Kola Peninsula: Evidence from Sm–Nd and U–Pb Isotopes. *Minerals* **2020**, *10*, 186. [[CrossRef](#)]
2. Mitrofanov, F.P.; Bayanova, T.B.; Ludden, J.N.; Korchagin, A.U.; Chashchin, V.V.; Nerovich, L.I.; Serov, P.A.; Mitrofanov, A.F.; Zhirov, D.V. Origin and Exploration of the Kola PGE-bearing Province. In *Ore Deposits: Origin, Exploration, and Exploitation*; Decrée, S., Robb, L., Eds.; John Wiley & Sons: Hoboken, NJ, USA, 2019; pp. 1–36.
3. Bayanova, T.; Ludden, J.; Mitrofanov, F. Timing and duration of Palaeoproterozoic events producing ore-bearing layered intrusions of the Baltic Shield: Metallogenic, petrological and geodynamic implications. *Geol. Soc. Lond. Spec. Publ.* **2009**, *323*, 165–198. [[CrossRef](#)]
4. Bayanova, T.B.; Rundquist, T.V.; Serov, P.A.; Korchagin, A.U.; Karpov, S.M. The Paleoproterozoic Fedorov–Pana Layered PGE complex of the northeastern Baltic Shield, Arctic Region: New U–Pb (baddeleyite) and Sm–Nd (sulfide) data. *Dokl. Earth Sci.* **2017**, *472*, 1–5. [[CrossRef](#)]
5. Bayanova, T.; Korchagin, A.; Mitrofanov, A.; Serov, P.; Ekimova, N.; Nitkina, E.; Kamensky, I.; Elizarov, D.; Huber, M. Long-lived mantle plume and polyphase evolution of palaeoproterozoic PGE intrusions in the fennoscandian shield. *Minerals* **2019**, *9*, 59. [[CrossRef](#)]
6. Jiang, S.Y.; Slack, J.F.; Palmer, M.R. Sm–Nd dating of the giant Sullivan Pb–Zn–Ag deposit, British Columbia. *Geology* **2000**, *28*, 751–754. [[CrossRef](#)]
7. Lodders, K. An experimental and theoretical study of rare-earth-element partitioning between sulfides (FeS, CaS) and silicate and applications to enstatite achondrites. *Meteorit. Planet. Sci.* **1996**, *31*, 749–766. [[CrossRef](#)]
8. Lüders, V.; Ziemann, M. Possibilities and limits of infrared light microthermometry applied to studies of pyrite-hosted fluid inclusions. *Chem. Geol.* **1999**, *154*, 169–178. [[CrossRef](#)]
9. Mao, G.; Hua, R.; Gao, J.; Li, W.; Zhao, K.; Long, G.; Lu, H. Existing forms of REE in gold-bearing pyrite of the Jinshan gold deposit, Jiangxi Province, China. *J. Rare Earths* **2009**, *27*, 1079–1087. [[CrossRef](#)]

10. Mills, R.A.; Elderfield, H. Rare earth element geochemistry of hydrothermal deposits from the active TAG Mound, 26° N Mid-Atlantic Ridge. *Geochim. Cosmochim. Acta* **1995**, *59*, 3511–3524. [[CrossRef](#)]
11. Morgan, J.W.; Wandless, G.A. Rare earth element distribution in some hydrothermal minerals: Evidence for crystallographic control. *Geochim. Cosmochim. Acta* **1980**, *44*, 973–980. [[CrossRef](#)]
12. Ni, Z.Y.; Chen, Y.J.; Li, N.; Zhang, H. Pb-Sr-Nd isotope constraints on the fluid source of the Dahu Au-Mo deposit in Qinling Orogen, central China, and implication for Triassic tectonic setting. *Ore Geol. Rev.* **2012**, *46*, 60–67. [[CrossRef](#)]
13. Rimskaya-Korsakova, M.N.; Dubinin, A.V. Rare earth elements in sulfides of submarine hydrothermal vents of the Atlantic Ocean Continental growth history of the river basin: Age distribution of detrital zircons from major rivers. *Dokl. Earth Sci.* **2003**, *389*, 432–436.
14. Wood, B.J.; Kiseeva, E.S. Trace element partitioning into sulfide: How lithophile elements become chalcophile and vice versa. *Am. Miner.* **2015**, *100*, 2371–2379. [[CrossRef](#)]
15. Yang, J.H.; Zhou, X.H. Rb-Sr, Sm-Nd, and Pb isotopes systematics of pyrite: Implications for the age and genesis of lode gold deposits. *Geology* **2002**, *29*, 711–714. [[CrossRef](#)]
16. Cao, Z.; Cao, H.; Tao, C.; Li, J.; Yu, Z.; Shu, L. Rare earth element geochemistry of hydrothermal deposits from Southwest Indian Ridge. *Acta Oceanol. Sin.* **2012**, *31*, 62–69. [[CrossRef](#)]
17. Jiao, Q.; Wang, L.; Deng, T.; Xu, D.; Chen, G.; Yu, D.; Ye, T.; Gao, Y. Origin of the ore-forming fluids and metals of the Hetai goldfield in Guangdong Province of South China: Constraints from C-H-O-S-Pb-He-Ar isotopes. *Ore Geol. Rev.* **2017**, *88*, 674–689. [[CrossRef](#)]
18. Li, D.; Chen, H.; Sun, X.; Fu, Y.; Liu, Q.; Xia, X.; Yang, Q. Coupled trace element and SIMS sulfur isotope geochemistry of sedimentary pyrite: Implications on pyrite growth of Caixiashan Pb–Zn deposit. *Geosci. Front.* **2019**, *10*, 2177–2188. [[CrossRef](#)]
19. Liu, K.; Yang, R.; Chen, W.; Liu, R.; Tao, P. Trace element and REE geochemistry of Sanshenjiang gold deposit, southeastern Guizhou Province, China. *Chin. J. Geochem.* **2014**, *33*, 109–118. [[CrossRef](#)]
20. Wang, S.; Li, H.; Zhai, S.; Yu, Z.; Cai, Z. Geochemical features of sulfides from the Deyin-1 hydrothermal field at the southern Mid-Atlantic Ridge near 15° S. *J. Ocean. Univ. China* **2017**, *16*, 1043–1054. [[CrossRef](#)]
21. Xu, L.; Yang, J.H.; Zeng, Q.D.; Xie, L.W.; Zhu, Y.S.; Li, R.; Li, B. Pyrite Rb-Sr, Sm-Nd and Fe isotopic constraints on the age and genesis of the Qingchengzi Pb-Zn deposits, northeastern China. *Ore Geol. Rev.* **2020**, *117*, 103324. [[CrossRef](#)]
22. Zeng, Z.; Ma, Y.; Yin, X.; Selby, D.; Kong, F.; Chen, S. Factors affecting the rare earth element compositions in massive sulfides from deep-sea hydrothermal systems. *Geochem. Geophys. Geosystems* **2015**, *18*, 1541–1576. [[CrossRef](#)]
23. Zhao, K.D.; Jiang, S.Y. Rare earth element and yttrium analyses of sulfides from the Dachang Sn-polymetallic ore field, Guangxi Province, China: Implication for ore genesis. *Geochem. J.* **2007**, *41*, 121–134. [[CrossRef](#)]
24. Liu, Y.C.; Song, Y.C.; Fard, M.; Zhou, L.M.; Hou, Z.Q.; Kendrick, M.A. Pyrite Re-Os age constraints on the Irankuh Zn-Pb deposit, Iran, and regional implications. *Ore Geol. Rev.* **2019**, *104*, 148–159. [[CrossRef](#)]
25. Tao, C.H.; Li, H.M.; Huang, W.; Han, X.Q.; Wu, G.H.; Su, X.; Zhou, N.; Lin, J.; He, Y.H.; Zhou, J.P. Mineralogical and geochemical features of sulfide chimneys from the 49°39' E hydrothermal field on the Southwest Indian Ridge and their geological inferences. *Chin. Sci. Bull.* **2011**, *56*, 2828–2838. [[CrossRef](#)]
26. Ruan, B.; Liao, M.; Sun, B.; Chen, C. Origin and nature of parental magma and sulfide segregation of the baixintan magmatic ni–cu sulfide deposit, southern central asian orogenic belt (Caob), nw china: Insights from mineral chemistry of chromite and silicate minerals. *Minerals* **2020**, *10*, 1050. [[CrossRef](#)]
27. Mitrofanov, F.P.; Bayanova, T.B.; Korchagin, A.U.; Groshev, N.Y.; Malitch, K.N.; Zhironov, D.V.; Mitrofanov, A.F. East Scandinavian and Noril'sk plume mafic large igneous provinces of Pd-Pt ores: Geological and metallogenic comparison. *Geol. Ore Depos.* **2013**, *55*, 305–319. [[CrossRef](#)]
28. Mints, M.V. 3D model of deep structure of the Early Precambrian crust in the East European Craton and paleogeodynamic implications. *Geotectonics* **2011**, *45*, 267–290. [[CrossRef](#)]
29. Mitrofanov, F.P. New Types of Mineral Raw Materials in the Kola Province: Discoveries and Perspectives. In *Smirnovsky Collection of Works*; VINITI RAS: Moscow, Russia, 2005; pp. 39–53.
30. Sharkov, E.V. *Formation of Layered Intrusions and Related Mineralization*; Scientific World: Moscow, Russia, 2006.
31. Bogatkov, O.A.; Kovalenko, V.I.; Sharkov, E.V. *Magmatism, Tectonics, and Geodynamics of the Earth*; Nauka: Moscow, Russia, 2010.
32. Smolkin, V.F.; Kremenetsky, A.A.; Vetrin, V.R. Geological and geochemical model of the Palaeoproterozoic ore-magmatic systems, Baltic Shield. *Natl. Geol.* **2009**, *3*, 54–62.
33. Naldrett, A.J. From the mantle to the bank: The life of a Ni-Cu-(PGE) sulfide deposit. *S. Afr. J. Geol.* **2010**, *113*, 1–32. [[CrossRef](#)]
34. Naldrett, A.J. *Magmatic Sulfide Deposits: Geology, Geochemistry and Exploration*; Springer: Berlin/Heidelberg, Germany, 2004; 746p.
35. Groves, D.I.; Vielreicher, R.M.; Goldfarb, R.J.; Condie, K.C. Controls on the heterogeneous distribution of mineral deposits through time. *Geol. Soc. Lond. Spec. Publ.* **2005**, *248*, 71–101. [[CrossRef](#)]
36. Karykowski, B.T.; Maier, W.D.; Groshev, N.Y.; Barnes, S.-J.; Pripachkin, P.V.; McDonald, I.; Savard, D. Critical Controls on the Formation of Contact-Style PGE-Ni-Cu Mineralization: Evidence from the Paleoproterozoic Monchegorsk Complex, Kola Region, Russia. *Econ. Geol.* **2018**, *113*, 911–935. [[CrossRef](#)]
37. Maier, W.D.; Hanski, E.J. Layered Mafic–Ultramafic Intrusions of Fennoscandia: Europe's Treasure Chest of Magmatic Metal Deposits. *Elements* **2017**, *13*, 415–420. [[CrossRef](#)]

38. Sharkov, E.V.; Chistyakov, A.V. Geological and petrological aspects of Ni-Cu-PGE mineralization in the early Paleoproterozoic Monchegorsk layered mafic-ultramafic complex, Kola Peninsula. *Geol. Ore Depos.* **2014**, *56*, 147–168. [[CrossRef](#)]
39. Yang, S.-H.; Hanski, E.; Li, C.; Maier, W.D.; Huhma, H.; Mokrushin, A.V.; Latypov, R.; Lahaye, Y.; O'Brien, H.; Qu, W.-J. Mantle source of the 2.44–2.50-Ga mantle plume-related magmatism in the Fennoscandian Shield: Evidence from Os, Nd, and Sr isotope compositions of the Monchepluton and Kemi intrusions. *Miner. Depos.* **2016**, *51*, 1055–1073. [[CrossRef](#)]
40. Hanski, E.; Huhma, H.; Smolkin, V.F.; Vaasjoki, M. The age of the ferropicritic volcanics and comagmatic Ni-bearing intrusions at Pechenga, Kola Peninsula, U.S.S.R. *Bull. Geol. Soc. Finl.* **1990**, *62*, 123–133. [[CrossRef](#)]
41. Sharkov, E.V.; Smolkin, V.F. The early Proterozoic Pechenga-Varzuga Belt: A case of Precambrian back-arc spreading. *Precambrian Res.* **1997**, *82*, 133–151. [[CrossRef](#)]
42. Walker, R.J.; Morgan, J.W.; Hanski, E.J.; Smolkin, V.F. Re-Os systematics of early proterozoic ferropicrites, Pechenga Complex, northwestern Russia: Evidence for ancient 187Os-enriched plumes. *Geochim. Cosmochim. Acta* **1997**, *61*, 3145–3160. [[CrossRef](#)]
43. Neradovsky, Y.; Alekseeva, S.; Chernousenko, E. Mineralogy and process properties of Kolvitsky titanomagnetite ore. *IOP Conf. Ser. Earth Environ. Sci.* **2019**, *262*, 12050. [[CrossRef](#)]
44. Voitekhovskiy, Y.L.; Neradovskiy, Y.N.; Grishin, N.N.; Rakitina, E.Y.; Kasikov, A. Kolvitsa field (geology, material composition of ores). *Vestn. MSTU* **2014**, *17*, 271–278.
45. Groshev, N.; Karykowski, B. The Main Anorthosite Layer of the West-Pana Intrusion, Kola Region: Geology and U-Pb Age Dating. *Minerals* **2019**, *9*, 71. [[CrossRef](#)]
46. Schissel, D.; Tsvetkov, A.A.; Mitrofanov, F.P.; Korchagin, A.U. Basal platinum-group element mineralization in the Federov Pansky Layered mafic intrusion, Kola Peninsula, Russia. *Econ. Geol.* **2002**, *97*, 1657–1677. [[CrossRef](#)]
47. Amelin, Y.V.; Heaman, L.M.; Semenov, V.S. U-Pb geochronology of layered mafic intrusions in the eastern Baltic Shield: Implications for the timing and duration of Paleoproterozoic continental rifting. *Precambrian Res.* **1995**, *75*, 31–46. [[CrossRef](#)]
48. Huhma, H.; Cliff, R.A.; Perttunen, V.; Sakko, M. Sm-Nd and Pb isotopic study of mafic rocks associated with early Proterozoic continental rifting: The Peräpohja schist belt in northern Finland. *Contrib. Mineral. Petrol.* **1990**, *104*, 369–379. [[CrossRef](#)]
49. Halkoaho, T.A.A.; Alapieti, T.T.; Lahtinen, J.J. The Sompujärvi PGE reef in the Penikat layered intrusion, northern Finland. *Mineral. Petrol.* **1990**, *42*, 39–55. [[CrossRef](#)]
50. Guice, G.L.; Törmänen, T.; Karykowski, B.T.; Johanson, B.; Lahaye, Y. Precious metal mineralisation in the Sotkavaara Intrusion, northern Finland: Peak Pt, Pd, Au and Cu offsets in a small intrusion with poorly-developed magmatic layering. *Ore Geol. Rev.* **2017**, *89*, 701–718. [[CrossRef](#)]
51. Iljina, M.; Maier, W.D.; Karinen, T. PGE-(Cu-Ni) Deposits of the Tornio-Näränkäväära Belt of Intrusions (Portimo, Penikat, and Koillismaa). In *Mineral Deposits of Finland*; Elsevier: Amsterdam, The Netherlands, 2015; pp. 133–164, ISBN 9780124104761.
52. Hanski, E.; Walker, R.J.; Huhma, H.; Suominen, I. The Os and Nd isotopic systematics of c. 2.44 Ga Akanvaara and Koitelainen mafic layered intrusions in northern Finland. *Precambrian Res.* **2001**, *109*, 73–102. [[CrossRef](#)]
53. Puchtel, I.; Brüggmann, G.; Hofmann, A.; Kulikov, V.; Kulikova, V. Os isotope systematics of komatiitic basalts from the Vetreny belt, Baltic Shield: Evidence for a chondritic source of the 2.45 Ga plume. *Contrib. Mineral. Petrol.* **2001**, *140*, 588–599. [[CrossRef](#)]
54. Vogel, D.C.; Vuollo, J.I.; Alapieti, T.T.; James, R.S. Tectonic, stratigraphic, and geochemical comparisons between ca. 2500–2440 Ma mafic igneous events in the Canadian and Fennoscandian Shields. *Precambrian Res.* **1998**, *92*, 89–116. [[CrossRef](#)]
55. Balashov, Y.A.; Bayanova, T.B.; Mitrofanov, F.P. Isotope data on the age and genesis of layered basic-ultrabasic intrusions in the Kola Peninsula and northern Karelia, northeastern Baltic Shield. *Precambrian Res.* **1993**, *64*, 197–205. [[CrossRef](#)]
56. Hanski, E.; Huhma, H.; Vaasjoki, M. Geochronology of northern Finland: A summary and discussion. *Spec. Pap. Geol. Surv. Finl.* **2001**, *33*, 255–279.
57. Lauri, L.S.; Mikkola, P.; Karinen, T. Early Paleoproterozoic felsic and mafic magmatism in the Karelian province of the Fennoscandian shield. *Lithos* **2012**, *151*, 74–82. [[CrossRef](#)]
58. Moilanen, M.; Hanski, E.; Konnunaho, J.; Yang, S.H.; Törmänen, T.; Li, C.; Zhou, L.M. Re-Os isotope geochemistry of komatiite-hosted Ni-Cu-PGE deposits in Finland. *Ore Geol. Rev.* **2019**, *105*, 102–122. [[CrossRef](#)]
59. Peltonen, P.; Brüggmann, G. Origin of layered continental mantle (Karelian craton, Finland): Geochemical and Re-Os isotope constraints. *Lithos* **2006**, *89*, 405–423. [[CrossRef](#)]
60. Melezhik, V.A.; Prave, A.R.; Fallick, A.E.; Hanski, E.J.; Lepland, A.; Kump, L.R.; Strauss, H. *Reading the Archive of Earth's Oxygenation*; Frontiers in Earth Sciences; Melezhik, V., Prave, A.R., Hanski, E.J., Fallick, A.E., Lepland, A., Kump, L.R., Strauss, H., Eds.; Springer: Berlin/Heidelberg, Germany, 2013; Volume 7.
61. Gorbunov, G.I.; Yakovlev, Y.; Goncharov, Y.; Gorelov, V.A.; Telnov, V.A. The nickel areas of the Kola Peninsula. *Bull.-Geol. Surv. Finl.* **1985**, *333*, 41–109.
62. Hickey, R.L.; Frey, F.A. Geochemical characteristics of boninite series volcanics: Implications for their source. *Geochim. Cosmochim. Acta* **1982**, *46*, 2099–2115. [[CrossRef](#)]
63. Bekker, A.; Grokhovskaya, T.L.; Hiebert, R.; Sharkov, E.V.; Bui, T.H.; Stadnek, K.R.; Chashchin, V.V.; Wing, B.A. Multiple sulfur isotope and mineralogical constraints on the genesis of Ni-Cu-PGE magmatic sulfide mineralization of the Monchegorsk Igneous Complex, Kola Peninsula, Russia. *Miner. Depos.* **2016**, *51*, 1035–1053. [[CrossRef](#)]
64. Chashchin, V.V.; Bayanova, T.B.; Mitrofanov, F.P.; Serov, P.A. Low-Sulfide PGE ores in paleoproterozoic Monchegorsk pluton and massifs of its southern framing, Kola Peninsula, Russia: Geological characteristic and isotopic geochronological evidence of polychronous ore-magmatic systems. *Geol. Ore Depos.* **2016**, *58*, 37–57. [[CrossRef](#)]

65. Raczek, I.; Jochum, K.P.; Hofmann, A.W. Neodymium and strontium isotope data for USGS reference materials BCR-1, BCR -2, BHV O-1, BHVO-2, AGV-1, AGV-2, GSP-1, GSP-2 and Eight MPI-DING refer ence glasses. *Geostand. Geoanalytical Res.* **2003**, *27*, 173–179. [[CrossRef](#)]
66. Tanaka, T.; Togashi, S.; Kamioka, H.; Amakawa, H.; Kagami, H.; Hamamoto, T.; Yuhara, M.; Orihashi, Y.; Yoneda, S.; Shimizu, H.; et al. JNdi-1: A neodymium isotopic reference in consistency with LaJolla neodymium. *Chem. Geol.* **2000**, *168*, 279–281. [[CrossRef](#)]
67. Elizarova, I.R.; Bayanova, T.B. Mass-spectrometric REE analysis in sulphide minerals. *J. Biol. Earth Sci.* **2012**, *2*, 45–49.
68. Dekov, V.M.; Kamenov, G.D.; Abrasheva, M.D.; Capaccioni, B.; Munnik, F. Mineralogical and geochemical investigation of seafloor massive sulfides from Panarea Platform (Aeolian Arc, Tyrrhenian Sea). *Chem. Geol.* **2013**, *335*, 136–148. [[CrossRef](#)]
69. Kong, P.; Deloule, E.; Palme, H. REE-bearing sulfide in Bishunpur (LL3.1), a highly unequilibrated ordinary chondrite. *Earth Planet. Sci. Lett.* **2000**, *177*, 1–7. [[CrossRef](#)]
70. Chen, G.; Shao, W.; Sun, D. *Genetic Mineralogy of Gold Deposits in Jiaodong Region with Emphasis on Gold Prospecting*; Chongqing Publishing House: Chongqing, China, 1989.
71. Serov, P.A.; Ekimova, N.A.; Bayanova, T.B.; Mitrofanov, F.P. Sulphide minerals as new Sm-Nd geochronometers for ore genesis dating of mafic-ultramafic layered intrusions of Baltic Shield. *Lithosphaera* **2014**, *4*, 11–21. (In Russian)
72. Zhitova, L.M.; Borovikov, A.A.; Gora, M.P.; Shevko, A.Y. Evolution trend of magmatogene fluids of the intercumulus crystallization stage of the Merensky Reef, Bushveld Complex, Republic of South Africa. *Dokl. Earth Sci.* **2009**, *429*, 1299–1304. [[CrossRef](#)]
73. Mansur, E.T.; Barnes, S.-J.; Duran, C.J. An overview of chalcophile element contents of pyrrhotite, pentlandite, chalcopyrite, and pyrite from magmatic Ni-Cu-PGE sulfide deposits. *Miner. Depos.* **2021**, *56*, 179–204. [[CrossRef](#)]
74. Wohlers, A.; Wood, B.J. Uranium, thorium and REE partitioning into sulfide liquids: Implications for reduced S-rich bodies. *Geochim. Cosmochim. Acta* **2017**, *205*, 226–244. [[CrossRef](#)]
75. Kotelnikov, A.E.; Kolmakova, D.A.; Kotelnikova, E.M. Determination of the copper-nickel ores formation sequence of the Kun-Manye deposit (Amur region). *Rudn. J. Eng. Res.* **2020**, *21*, 48–57. [[CrossRef](#)]
76. Raič, S.; Krenn, K.; Mogessie, A. Possible sources for CH<sub>4</sub>-rich fluid inclusions in olivine from troctolitic rocks of the Bathtub intrusion, Duluth Complex, U.S.A. *Precambrian Res.* **2019**, *331*, 105376. [[CrossRef](#)]
77. Aibai, A.; Deng, X.; Pirajno, F.; Han, S.; Liu, W.; Li, X.; Chen, X.; Wu, Y.; Liu, J.; Chen, Y. Origin of ore-forming fluids of Tokuzbay gold deposit in the South Altai, northwest China: Constraints from Sr-Nd-Pb isotopes. *Ore Geol. Rev.* **2021**, *134*, 104165. [[CrossRef](#)]
78. Cao, H.; Sun, Z.; Jiang, Z.; Dong, A.; Geng, W.; Zhang, X.; Li, X.; Yan, D.; Liu, W. Source origin and ore-controlling factors of hydrothermal sulfides from the Tianzuo hydrothermal field, Southwest Indian Ridge. *Ore Geol. Rev.* **2021**, *134*, 104168. [[CrossRef](#)]
79. Shelton, K.L.; Cavender, B.D.; Perry, L.E.; Schiffbauer, J.D.; Appold, M.S.; Burstein, I.; Fike, D.A. Stable isotope and fluid inclusion studies of early Zn-Cu-(Ni-Co)-rich ores, lower ore zone of Brushy Creek mine, Viburnum Trend MVT district, Missouri, U.S.A.: Products of multiple sulfur sources and metal-specific fluids. *Ore Geol. Rev.* **2020**, *118*, 103358. [[CrossRef](#)]